Spectroscopy 19 (2005) 147–164
IOS Press

Enhancing infrared response of adsorbed biomaterials using ellipsometry and textured surfaces

Daniel W. Thompson * and John A. Woollam
University of Nebraska-Lincoln Electrical Engineering Department, 209N WSEC, Lincoln, NE 68588-0511, USA

Abstract. Infrared spectra are of interest for numerous applications because of the chemical bond information present in the absorption characteristics. Obtaining meaningful infrared spectra from monolayers adsorbed to surfaces can be difficult because of the small amount of material being probed. For instance, it is often of interest to probe adsorbates on a surface after exposure to a protein solution. Use of textured (patterned) surfaces to increase the mass of material sensed is expected to enhance these spectra. Here the infrared ellipsometric enhancement is calculated for a layer of adsorbate on a number of proposed nanostructured surfaces to predict which is most advantageous for obtaining infrared spectra. The approach used here could also be applied to other adsorbates by optimizing the pattern dimensions for different sizes. It also works for visible spectroscopy as long as pattern dimensions are significantly smaller than the wavelength. The effect of using these structures (rods, wells, and trenches) is compared to the response of flat metal or dielectric surfaces over a range of incidence angles of the infrared beam. Predicted sensitivities are based on the calculated effect of adsorbate on intensities in an ellipsometric measurement. Trench structures appear to have significant advantages both in sensitivity and ability to distinguish adsorbed species orientation.

Keywords: Infrared, ellipsometry, protein

1. Introduction

Monolayers of biomaterials attached to surfaces often yield only weak infrared responses. One strategy to increase detectability of these materials is to enhance the surface area, increasing the mass of the adsorbed species available for probing [1,11,14,15]. This is especially useful for optical techniques for which the probe penetration depth is much greater than the thickness of an adsorbed layer. This surface enhancement can be accomplished by lithography or other patterning techniques, roughening by bombardment, or texturing by electrochemical methods. The last category includes materials such as porous silicon and porous alumina, which have varying degrees of order in their microstructure [4,16].

The present work analyzes ellipsometric signal enhancement due to increasing the uptake of proteins on textured surfaces. The same approach can be applied to other adsorbates such as toxins or biowarfare agents. The focus here is on the use of patterned structures to enhance the measurability of infrared absorption peaks. Previous work used visible ellipsometry and radioactive labeling to observe a factor of 70 increase in protein uptake in porous silicon compared to planar silicon [15]. The same group also published work using IR ellipsometry to observe the absorption spectrum of human carbonic anhydrase II

*Corresponding author. Tel.: +1 402 326 8081; Fax: +1 402 472 4732; E-mail: dthompson2@unl.edu.

in porous silicon. Amide I absorption peaks at nine separate frequencies were identified using a second-derivative technique [14,15]. A shift of characteristic frequencies from book values [21] was noted and attributed to the fact that the protein is no longer in solution. Such changes of absorption behavior due to environment are likely to be an ongoing challenge in such studies. Porous silicon, however, has a less ordered character than patterned surfaces, and it is not clear to what extent this disorder will affect the ability to functionalize it to attract particular species. For this reason, the present work is limited to surfaces on which nanostructure is more directly controlled by fabrication.

2. Ellipsometry and the dielectric function

Ellipsometry, the measurement of how the polarization state of a light beam is transformed by interaction with a sample [3], can be extremely sensitive to the dielectric properties of surfaces and their overlayers. When light with a known polarization state is incident on a surface at an oblique angle, the incident and emergent beams form a plane of incidence. Maxwell's equations predict the dependence of the reflected state on the complex dielectric function of each material, $\varepsilon(\sigma) = \varepsilon_1(\sigma) + i\varepsilon_2(\sigma)$, where frequency σ is the reciprocal of the wavelength. This is often expressed as the complex index of refraction $n(\sigma) = \sqrt{\varepsilon(\sigma)}$. The polarization state is defined by the relationship of the magnitude and phase of the electric field components parallel and perpendicular (denoted by p and s, respectively) to the plane of incidence. Ellipsometry measures the complex ratio of the electric field reflection coefficients R_p and R_s:

$$\frac{R_p}{R_s} = \tan\psi \exp(i\Delta), \tag{1}$$

where ψ and Δ are used conventionally to express the magnitude and phase of the ratio. An optical model containing thickness and $\varepsilon(\sigma)$ for each layer is used to compare calculated $\psi(\sigma)$ and $\Delta(\sigma)$ values to those obtained by experiment; unknowns in the model are adjusted using a computer algorithm to minimize the difference [13,25].

In general, $\varepsilon(\sigma)$ is a tensor which depends on the direction of the electric field. This dependence can be induced by asymmetry of any type on a scale significantly smaller than the wavelength. In this paper, both atomic-scale and nanoscale asymmetries are considered in predicting ε. As long as these asymmetries align to a coordinate system defined by the plane of incidence and the sample surface, there is no p–s conversion and generalized ellipsometry is not necessary [20,24].

3. Proposed structures

The structures proposed were evaluated according to the surface area enhancement they afford. If protein adsorption to a planar surface is in practice limited to a monolayer due to a lack of cohesion (affinity for itself), the amount of protein which may be "condensed" on the surface is proportional to the available surface area. Even in cases where multiple protein layers can be formed, such surface enhancement is desirable. Geometrically enhancing the surface area by patterning structures in it should then aid in detecting the adsorbate. Another enhancement scheme, not dealt with here, is increasing the electric field strength in the protein film by introducing single or multiple-layer dielectric stacks on the substrate before adsorption.

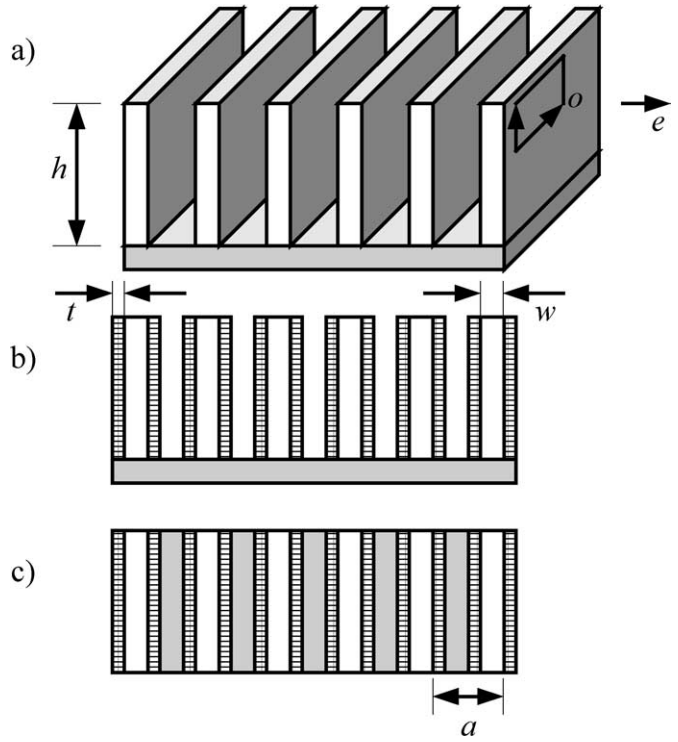

Fig. 1. Schematic diagram of trench structure. (a) Isometric view with no protein. (b) Side view. Hatched areas represent orientation of adsorbate. (c) Top view.

The proposed geometric enhancements were analyzed using structures with and without adsorbed protein, as shown in Figs 1–3. For comparison, responses to adsorption on flat dielectric (silicon) and flat metallic (aluminum) substrates were also calculated. The structures are defined in terms of characteristic dimensional parameters, and calculations were performed using dimensions that can be readily fabricated. Actual performance is strongly dependent on these sizes, since structures having lower density of substrate material can more efficiently use the space for protein. The structure-based anisotropy induced by patterning was modeled by setting the appropriate depolarization factors in an effective-medium approximation [8]. These factors are explained in a separate publication [23]. Note that the effective-medium ordinary plane and extraordinary direction ('o' and 'e') for the structure anisotropy depend on symmetry, as marked in each figure.

The calculations were performed assuming a uniaxial geometry for the protein, since most proteins are not entirely symmetrical, such as human serum albumin, shown in Fig. 4 [5]. As long as the attachment orientation is consistent with respect to the surface, random orientation in the plane of the surface results in effectively uniaxial anisotropy [19]. This can always be simplified to be an isotropic adsorbate for cases where proteins attach with totally random orientations. All structures studied here consist of "vertical" walls, with all surface normals lying in the plane of the original surface. The adsorption on the top and bottom horizontal surfaces, a relatively small contribution to the total signal, was ignored for the textured surfaces. Spongelike porosity (e.g., porous silicon) and logpile structures [18] introduce non-vertical surfaces which increase surface area enhancement, but are not covered here due to fabrication concerns. This also randomizes the orientation of the adsorbate and reduces sensitivity to its anisotropy.

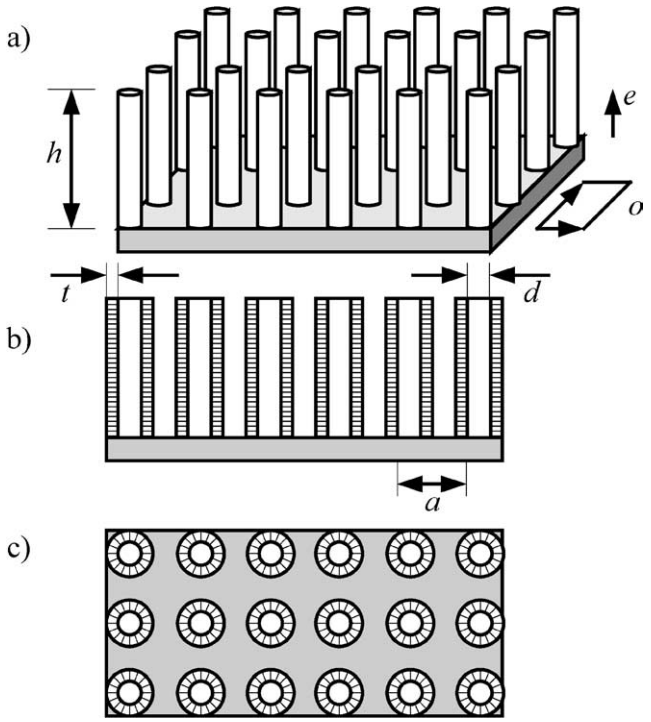

Fig. 2. Diagram of rod geometry. (a) Isometric view with no protein. (b) Side view with protein. (c) Top view.

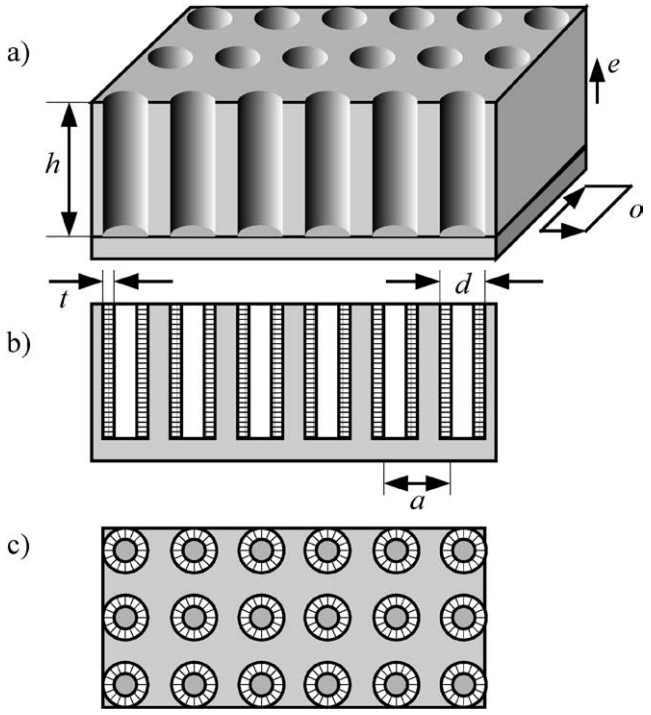

Fig. 3. Diagram of well geometry. (a) Isometric view with no protein. (b) Side view with protein. (c) Top view.

Fig. 4. Human serum albumin. The shape is somewhat flat, indicating that it may not be likely to attach to surfaces in random orientation. The secondary structure, shown by color, is strongly α-helical (green).

The first structure considered is the trench (Fig. 1), which is simply composed of parallel walls of width w, period a, and height h. The vertical surface area available for adsorption is directly proportional to the well depth and inversely proportional to a. These enhancements are independent of w, which puts a lower limit on a. Finally, the interior spacing $(a - w)$ must be large enough to accomodate three times the adsorbate thickness and allow enough mobility for adsorbates to access the deeper parts of the structure. Fabrication considerations limit the aspect ratio h/w. In all cases radii of curvature are ignored here. The surface area enhancement ratio is defined by selecting a representative region ("unit cell") of the surface and rationing the new surface area with the pattern to that of the original flat surface:

$$\rho = \frac{\text{surface area available for adsorption}}{\text{unpatterned surface area}} = 2\frac{h}{a}. \tag{2}$$

This quantity gives the maximum mass uptake advantage of using the enhanced surface; the increase in ellipsometric signal, calculated via modeling, is shown in the next section.

If allowed to extend beyond the thickness limits, these walls would become a set of infinite parallel planes with normal vector parallel to the surface of the sample. For this reason, the trench has structure-based uniaxial anisotropy with the optic axis in the plane of the sample and perpendicular to the trench walls, resulting in the o and e designations in the figure. The adsorbed material has anisotropy with the same orientation. For all calculations here, the response was determined for the case where the optic axis is in the plane of incidence (x-direction), as well as perpendicular to it (y-direction). Bruggeman effective medium theory predicts the dielectric function in each direction from symmetry considerations and volume fractions of each material [8].

For calculation purposes, the volume fraction of each constituent is used in the modelling software. For trenches these are w/a and $2t/a$ (two adsorbed layers per trench) for the solid and adsorbate fractions, respectively. The void fraction is the remaining amount, or $1-(w+2t)/a$.

The second proposed structure is an array of rods, characterized by diameter d, center-to-center spacing a and height h. The surface area enhancement ratio in this case is

$$\begin{aligned} \rho &= \frac{\pi dh}{a^2} \quad \text{square array,} \\ \rho &= \frac{2\pi dh}{\sqrt{3}a^2} \quad \text{hexagonal array.} \end{aligned} \tag{3}$$

If the rod structure is scaled laterally, d and a vary proportionally, so the net effect is an inverse relationship between ρ and a. Note that since $d < a$, the maximum enhancement (hexagonal array) is a factor $\pi/\sqrt{3}$ ($= 1.82$) larger than that of the trench with similar dimensions. This has structure-based anisotropy with optic axis normal to the original surface. The adsorbate, however, orients with its optic axis parallel to the original surface in all possible directions (Fig. 2c). Schubert [20] has shown that the effective ordinary and extraordinary dielectric functions for the adsorbate itself is given by

$$\begin{aligned} \varepsilon_{o,\text{eff}} &= \frac{1}{2}[\varepsilon_o + \varepsilon_e], \\ \varepsilon_{e,\text{eff}} &= \varepsilon_o, \end{aligned} \tag{4}$$

where ε_o and ε_e are the intrinsic ordinary and extraordinary dielectric functions. *The effective optic axis for the adsorbate then coincides with that of the structural anisotropy*, but the intrinsic 'o' properties contribute to both 'e' and 'o' components of the effective dielectric function. The effective 'e' dielectric function is that of the intrinsic 'o'. The optical model for such a layer is then modeled as a uniaxial material composed of two effective media, each with three components: substrate material, void, and one of the effective adsorbate dielectric functions. The depolarization factor is set to 0.5 in the plane of the sample and zero perpendicular, consistent with columnar geometry [7]. The volume fractions are

$$\left.\begin{aligned} r_m &= \frac{\pi d^2}{4a^2} \\ r_a &= \frac{\pi}{4a^2}(d+t)^2 - r_m = \frac{\pi}{4a^2}(2dt+t^2) \end{aligned}\right\} \text{square array,}$$

$$\left.\begin{aligned} r_m &= \frac{\pi d^2}{2\sqrt{3}a^2} \\ r_a &= \frac{\pi}{2\sqrt{3}a^2}(2dt+t^2) \end{aligned}\right\} \text{hexagonal array,} \tag{5}$$

$$r_v = 1 - r_m - r_a,$$

where subscripts m, a, and v refer to the matrix, adsorbate, and void, respectively.

The final proposed structure is an array of circular wells, where d is the diameter of the well. The enhancement is similar to that of the towers, with the maximum enhancement matching that of the rod

structure with similar parameters. The anisotropy is handled in a similar fashion. The volume fractions are

$$\left.\begin{aligned} r_v &= \frac{\pi}{4a^2}(d-t)^2 \\ r_a &= r_v - \frac{\pi}{4a^2}d^2 = \frac{\pi}{4a^2}(t^2-2dt) \end{aligned}\right\} \text{ square array,}$$

$$\left.\begin{aligned} r_v &= \frac{\pi}{2\sqrt{3}a^2}(d-t)^2 \\ r_a &= \frac{\pi}{2\sqrt{3}a^2}(t^2-2dt) \end{aligned}\right\} \text{ hexagonal array,} \tag{6}$$

$$r_m = 1 - r_v - r_a.$$

As the diameter of the wells decreases, approaching the size of the adsorbate, the surface area cannot be utilized as efficiently. This is not the case in the rod structure, but its limitation is that there must be space for the adsorbate to move to the lower parts of the structure. For near-spherical adsorbates, this requires a spacing of three times the adsorbate size t between rods, or $a \geqslant d + 3t$. This spacing could be reduced to double if the adsorbate is mobile on the surface.

4. Simulations and discussion

To perform realistic simulations of optical response, dimensions must be chosen that can be readily fabricated. One group working on photonic crystals has fabricated rod structures using deep reactive ion etching with 5-μm depth, 205-nm diameter, and 570-nm period [6]. Though these dimensions are only marginally small enough to be appropriate for the effective medium approximation at $\lambda = 5$ μm, they provide a conservative estimate of the achievable dimensions, since smaller sizes generally enhance performance. Here we will set $a = 570$ nm, $h = 5$ μm, and use 205 nm as a minimum thickness for structural integrity. Common protein sizes are in the range 5 to 50 nm, so the requirement for spacings between features of $3t$ is always fulfilled for these dimensions.

Electrochemically fabricated porous alumina has columnar pores that resemble the well structure [10,17,23]. The dimensions in this case are somewhat smaller, with typical lattice parameters on the order of 100 nm. Void fraction can be effectively engineered by isotropically etching the pores to increase diameter. The ordering tends toward hexagonal symmetry. The adsorption layer is composed of a porous dielectric formed from a metal substrate. This is optically different from the silicon structures, where the patterned layer and substrate are the same material.

Two unpatterned samples were simulated for the purpose of comparing ellipsometric responses of adsorbed proteins on textured surfaces with those on simple planar surfaces. Planar silicon is dielectric in the spectral range of interest, with a relatively high ε ($\cong 11.8$). Planar aluminum is used as an example of a reflective substrate. Although surface oxides cause a modest change the ellipsometric response, they are not included in the simulation for the planar cases because these effects do not interfere significantly with the response due to the adsorbate.

The calculated magnitude of the ellipsometric effect is only meaningful when compared to the noise level of the data in a particular instrument. Figure 5 shows a difference plot of ψ and Δ for two successive

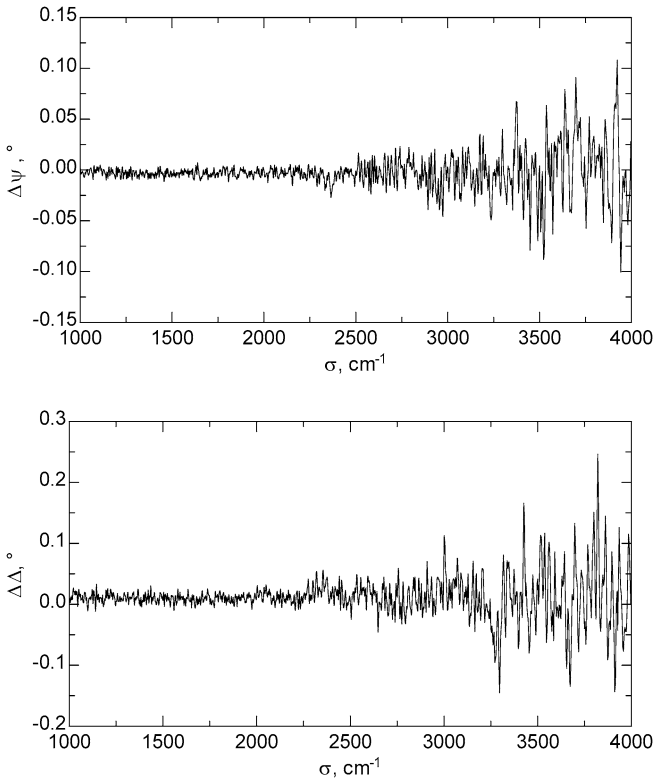

Fig. 5. Difference in ψ and Δ for two successive identical scans on aluminum. This illustrates the noise level achievable with the current IRSE.

Table 1
Dimensions (nm) of various geometric structures

	w	h	t	d	a	r_v	r_m	r_a	ρ
Trench	205	5000	10		570	0.605	0.360	0.035	17.5439
Rod		5000	10	205	570	0.888	0.102	0.010	9.9111
Well		5000	10	365	570	0.305	0.678	0.017	17.6467
Porous		1000	10	80	100	0.385	0.497	0.118	25.1327

$\rho \equiv$ surface area enhancement ratio; $r \equiv$ volume fraction. Both ρ and r are dimensionless.

identical scans of an aluminum sample, illustrating the noise level for a three-hour scan with a liquid-nitrogen cooled mercury cadmium telluride (MCT) detector on our infrared ellipsometer. Noise levels are estimated to be 0.01° for ψ and 0.02° for Δ at a resolution of 4 cm^{-1} in the range from 1000 to 4000 cm^{-1}.

Parameters for our simulations are shown in Table 1, calculated from the expressions and parameters given in the previous section. Square arrays were used for all simulations, based on an example of a silicon rod structure found in the literature [6] and the fact that porous arrays are not always perfectly hexagonal. The difference between hexagonal and square arrays is less than 20% in ρ, a relatively small factor compared to the enhancement ratios being analyzed. The final column in the table shows surface area enhancement ratio, but the exact numbers in the table should be deemphasized, as values for w, d,

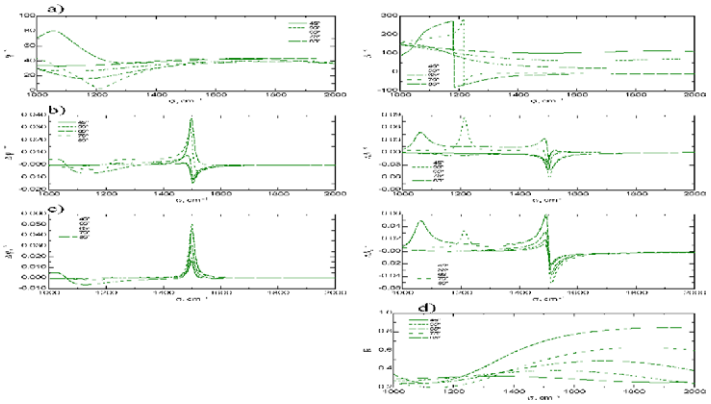

Fig. 6. Dielectric properties for absorbing and transparent hypothetical adsorbate with a single absorption peak. For the transparent case, $\varepsilon_2 = 0$.

and a have been chosen based on current fabrication capabilities. Since these capabilities will inevitably improve with time, the simulations shown are a conservative estimate of future possibilities.

Despite the increased dimensionality of the rod and well structures, they actually provide protein capture capability very similar to trenches, with the parameters shown. Feature size reductions result in greater performance benefit for two-dimensional structures, as shown for the porous material. A smaller thickness d was chosen for the porous material, as the surfaces are less accessible for the adsorbate than for the structures with larger dimensions. This kept the enhancement ratios comparable to those of the other structures. The adsorbate volume fraction was considerably higher for the porous material.

Three cases will be compared for each surface: isotropic, no absorption (case A); uniaxial, absorption in the intrinsic ordinary dielectric function ε_o (case B); uniaxial, absorption in intrinsic extraordinary component ε_e (case C). These intrinsic dielectric functions (tensor elements, functions of frequency σ, in cm^{-1}) are related in Eq. (4) to the effective properties $\varepsilon_{o,\text{eff}}$ and $\varepsilon_{e,\text{eff}}$ due to orientation averaging. Two sets of difference plots ($\psi_B - \psi_A$, $\Delta_B - \Delta_A$, $\psi_C - \psi_A$, $\Delta_C - \Delta_A$) result from these spectra to show the effect of absorption in each direction. If the effect of absorption produces significantly different shapes for the e- and o-components, this implies the two sets of dielectric functions can be determined independently, yielding new information on molecule anisotropy. Dielectric functions for the hypothetical adsorbate in the spectral range of interest are shown in Fig. 6. For the case of no absorption, a dielectric constant of 2.56 was used, a value found for protein in previous work by Arwin et al. [1]. For cases with absorption, a single Lorentzian oscillator term [26] was added to the dispersion model, with a peak ε_2 of 0.15, center frequency of 1500 cm^{-1}, and broadening of 20 cm^{-1}. The height was chosen to be one order of magnitude smaller than the peak ε_2 from Arwin's work, to account for the fact that distinguishing between proteins or other biomolecules will require detection of minor as well as major absorption peaks.

To demonstrate the difficulty of using the conventional ellipsometric parameters ψ and Δ for sensitivity calculations, graphs of simulation results for the silicon rod structure at five angles of incidence are shown in Fig. 7. The ellipometric spectra are shown for case A. Difference plots (case B minus case A) for absorption in ε_o are shown next, followed by similar plots for absorption in ε_e (case C minus case A). Because ellipsometric precision is also dependent on the magnitude of the reflected intensity, a graph of this quantity for the case of input radiation with equal components of s- and p-polarization is also included.

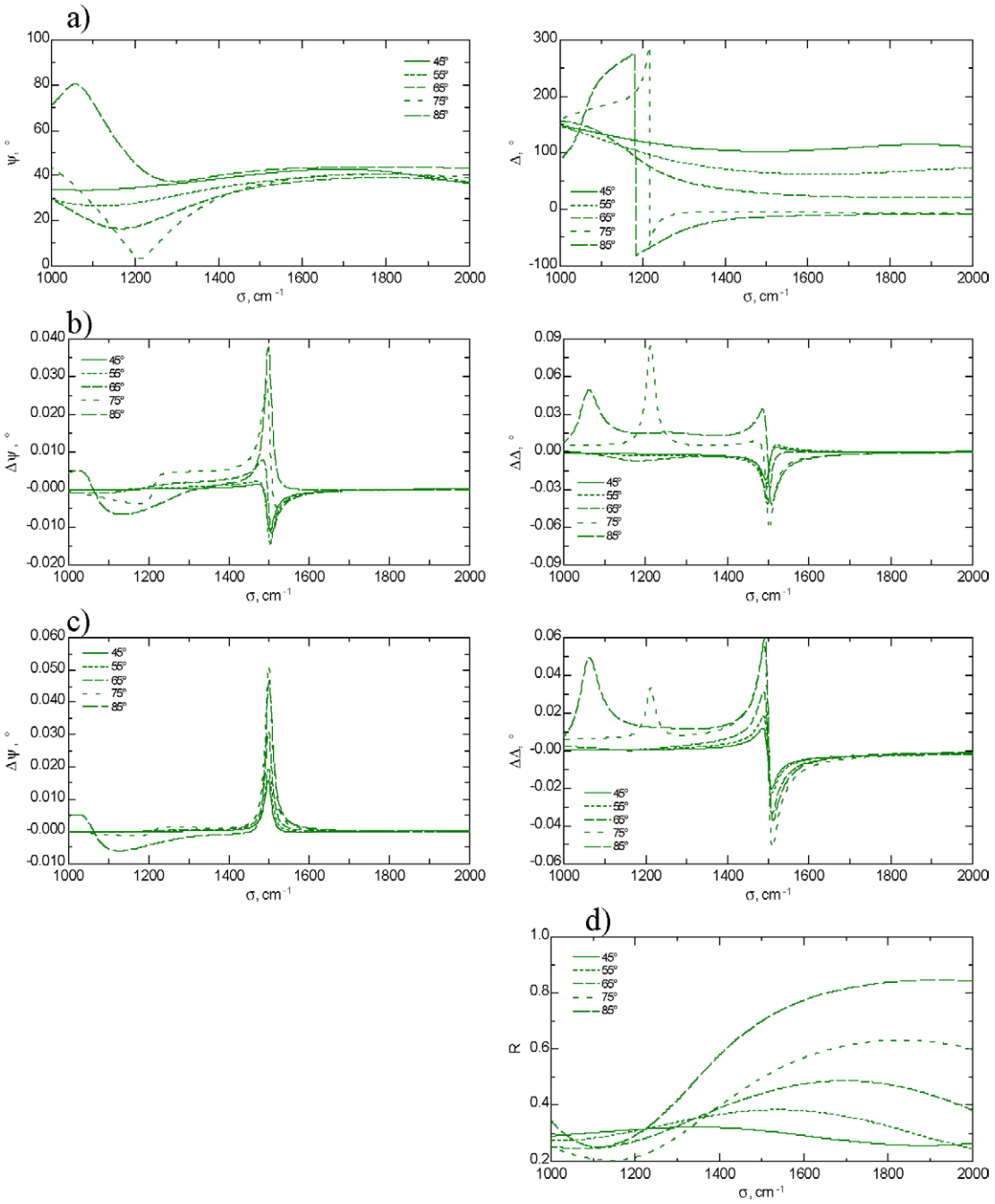

Fig. 7. Simulation results for protein adsorbed to a silicon rod structure. (a) Ellipsometric spectra for case A. (b) Ellipsometric difference plot (case B – case A). (c) Ellipsometric difference plot (case C – case A). (d) Intensity reflection for input radiation with s- and p-polarized components of equal magnitude (case A).

Areas of apparent enhanced sensitivity in ψ and Δ with low reflection do not necessarily represent improved detection capability because the small signal will result in increased noise. Values of ψ near 0° and 90°, as seen in the figure near 1060 and 1210 cm^{-1}, also imply that Δ will be more difficult to measure precisely, since one reflected component is very small and its phase will be difficult to determine. For these reasons, the presence of a peak in a difference plot due to one of these conditions will be referred to as *illusory* sensitivity. This phenomenon has sometimes been ignored in sensitivity calculations [2], but in other cases has been taken into account [12].

To avoid illusory sensitivity peaks, it is better to calculate the effect of adsorbate on the intensity measurements that lead to the ellipsometric parameters. While the ψ–Δ representation is a convenient description of the field behavior of the light, a more useful representation is based on the changes in measured intensity when either the polarization state of the incident light or the polarization sensitivity of the detector is changed [9]. The parameters are derivable from ψ and Δ according to

$$\begin{aligned} N &= \cos 2\psi, \\ C &= \sin 2\psi \cos \Delta, \\ S &= \sin 2\psi \sin \Delta. \end{aligned} \tag{7}$$

If R is the intensity reflection, assuming an input state with equal components of s- and p-polarized light, sensitivity calculations can then be based on the changes in N, C, and S due to molecule absorption multiplied by the reflectance: $R\Delta N$, $R\Delta C$, and $R\Delta S$. These quantities are proportional to changes in reflected intensity measured by the ellipsometer due to small differences in optical model parameters. This simplifies interpretation of the results by eliminating features due to illusory sensitivity.

The sensitivity of a particular ellipsometer system to N, C, and S is important to consider. A simple rotating analyzer ellipsometer (RAE) has no sensitivity to S, and a simple phase modulation ellipsometer (PME) no sensitivity to N. These limitations can be overcome by the use of a variable retarder for RAE and an extra polarizer position for PME. Rotating compensator ellipsometer (RCE) systems have roughly equal sensitivity to all three, depending on the actual value of the compensator retardance. The simulations presented here can generally be used in conjunction with either RCE or RAE with a variable retarder, so all three quantities will be weighted equally.

Based on the above considerations, an improved sensitivity figure of merit is

$$FOM = \sqrt{(R\Delta N)^2 + (R\Delta C)^2 + (R\Delta S)^2}, \tag{8}$$

which gives an indication of the fraction of the incident power affected by adsorbate absorption. Figures 8–14 show this quantity for selected structures described in the previous section. Use of this new figure of merit simplifies the analysis by reducing the number of graphs for each structure to two: one each for the effects of absorption in ε_o and ε_e. A discussion of the findings follows.

Although *FOM* eliminates many illusory sensitivity features, it also suppresses some information which is better seen in the lineshapes of $R\Delta N$, $R\Delta C$, and $R\Delta S$.

Flat silicon. This provides a reference point to evaluate the advantages of silicon structures. Sensitivity appears to be generally near the noise level with the best sensitivities to absorption in ε_o and ε_e coming near the silicon brewster angle ($\sim$73.4°). It should also be noted that the response for absorption in the ordinary direction is similar in shape to and in the opposite direction (in $R\Delta N$, $R\Delta C$, and $R\Delta S$, not

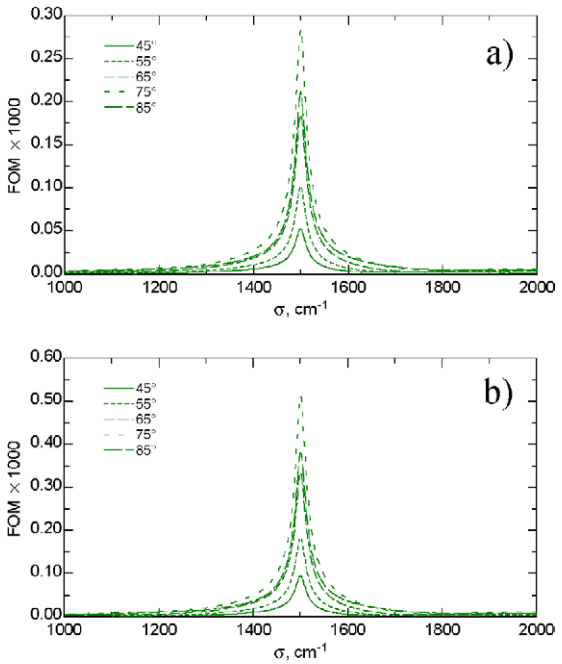

Fig. 8. Figure of merit at five incidence angles for a flat silicon substrate. (a) Response to absorption in the ordinary dielectric function of the adsorbate (case B − case A). (b) Response to absorption in the extraordinary dielectric function of the adsorbate (case C − case A).

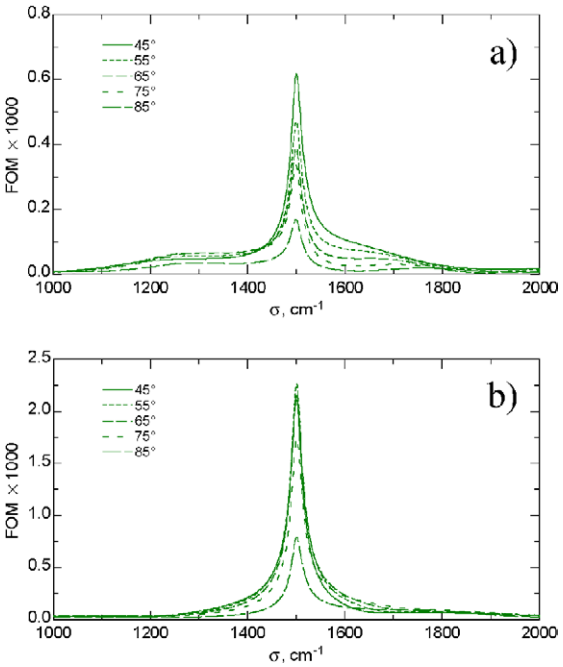

Fig. 9. Figure of merit at five incidence angles for trenches patterned in silicon. The trench walls are oriented with their surface normals in the plane of incidence. (a) Response to absorption in the ordinary dielectric function of the adsorbate (case B − case A). (b) Response to absorption in the extraordinary dielectric function of the adsorbate (case C − case A).

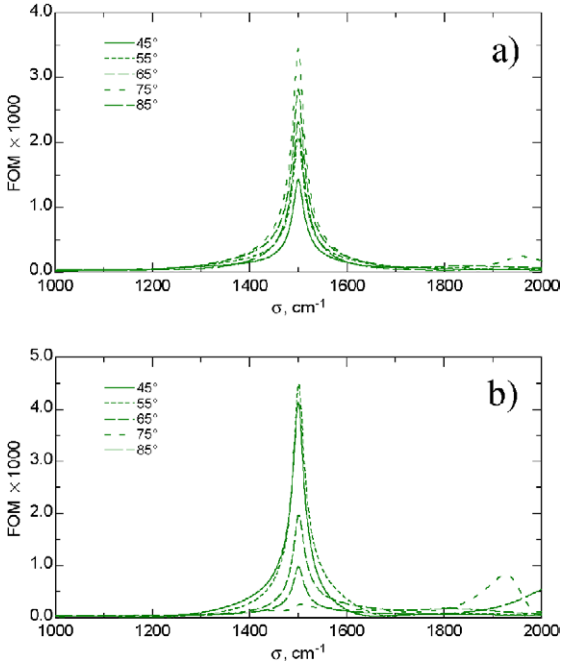

Fig. 10. Figure of merit at five incidence angles for trenches patterned in silicon. The trench walls are oriented with their surface normals perpendicular to the plane of incidence. (a) Response to absorption in the ordinary dielectric function of the adsorbate (case B − case A). (b) Response to absorption in the extraordinary dielectric function of the adsorbate (case C − case A).

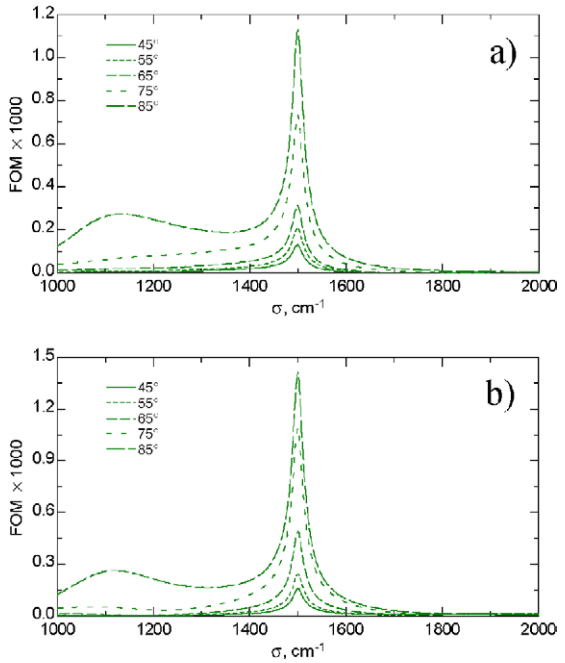

Fig. 11. Figure of merit at five incidence angles for rods patterned in silicon. (a) Response to absorption in the ordinary dielectric function of the adsorbate (case B − case A). (b) Response to absorption in the extraordinary dielectric function of the adsorbate (case C − case A).

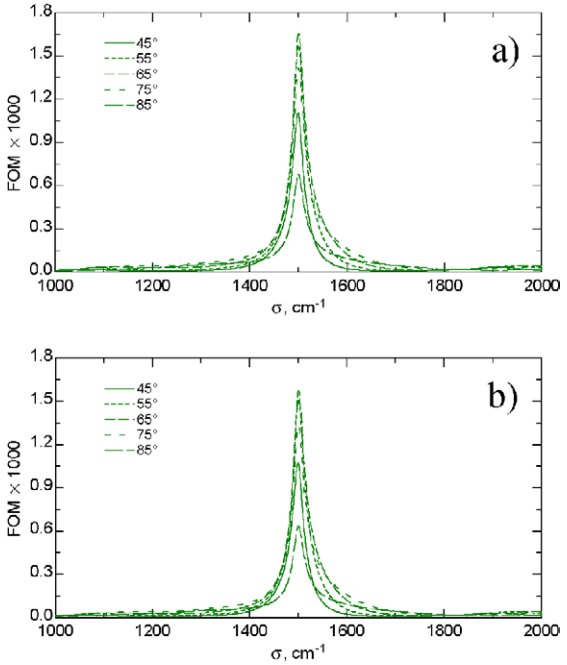

Fig. 12. Figure of merit at five incidence angles for wells patterned in silicon. (a) Response to absorption in the ordinary dielectric function of the adsorbate (case B − case A). (b) Response to absorption in the extraordinary dielectric function of the adsorbate (case C − case A).

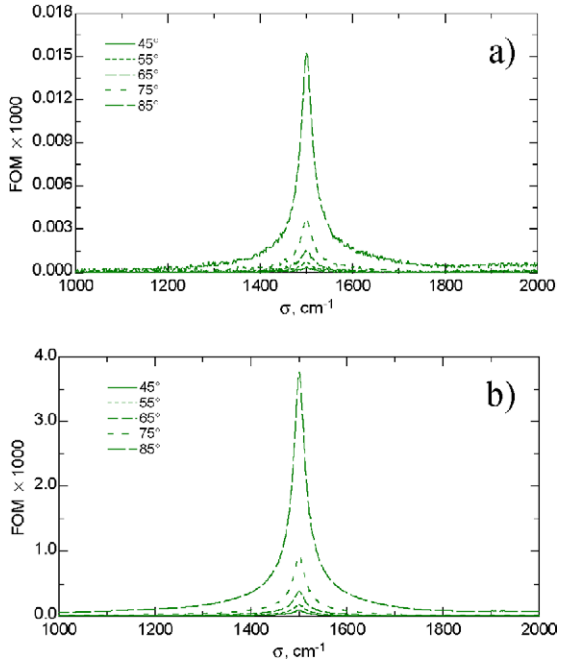

Fig. 13. Figure of merit at five incidence angles for a flat aluminum substrate. (a) Response to absorption in the ordinary dielectric function of the adsorbate (case B − case A). (b) Response to absorption in the extraordinary dielectric function of the adsorbate (case C − case A).

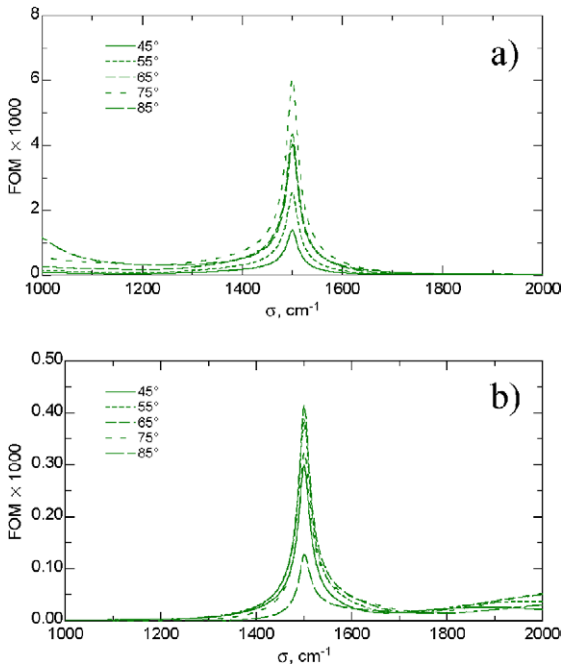

Fig. 14. Figure of merit at five incidence angles for porous alumina. (a) Response to absorption in the ordinary dielectric function of the adsorbate (case B − case A). (b) Response to absorption in the extraordinary dielectric function of the adsorbate (case C − case A).

shown) of that for the extraordinary direction, but about half the magnitude. This means that the orientation of spectrally isolated ε_o absorptions can be determined, but it would not be possible to distinguish ε_e absorptions from isotropic ones. The response for isotropic absorption, a sum of the two component responses, is actually less than for those in ε_e. Though a major absorption would be identifiable, finer features such as bandshapes of overlapping peaks would be difficult to determine.

Trenches. The trench structure has the advantage of being observable in various orientations. Figures 9 and 10 illustrate two of the most obvious possibilities: trenches parallel and perpendicular to the plane of incidence, respectively. The shape of the response in *FOM* is very similar to that of flat silicon. However, response to ε_o absorption is shaped quite differently, implying that the orientation of an adsorbate molecule can be determined. The dependence of the response on incidence angle also helps distinguish absorptions in ε_e and ε_o. Values of *FOM* greater than 10^{-3} represent a significant increase in detectibility compared to flat silicon, but probably a little less than the factor of 18 increase in surface area.

An intriguing feature is seen in Fig. 10b (wall surface normals perpendicular to plane of incidence) for the ε_o response at 75° incidence angle. The *FOM* exhibits a maximum of significant width and height at 1920 cm^{-1}, a region where the ε changed very little (Fig. 6). This suggests that tuning the incidence angle or the thickness of the capture layer may be beneficial for signal enhancement.

The two orientations of the trenches also generally exhibit responses of *opposite sign*, which indicates that using both measurements will indeed enhance sensitivity to adsorbed materials. This is a key advantage of the trench structure.

Rods and wells. These two structures are treated together because the optical model is identical for these two cases, with adjustment only for volume fractions. The rod structure has the lowest ρ of the

structures investigated, and correspondingly low response magnitudes. Increasing the diameter of the rods would cause the response to eventually approach that of the well structure. Both structures exhibit modest sensitivities and little distinction between the ε_o and ε_e responses.

The rod structure also has a region ($\sim$1100 cm^{-1}) of enhanced response despite very small changes in ε. Further investigation is required to determine whether this effect can be made large enough to capitalize on. Preliminarily, the trench structure appears to have significant advantages both in sensitivity and ability to distinguish adsorbed species orientation.

Flat aluminum. This surface is representative of reflective metallic surfaces in general. The response characteristic is relatively simple, with almost no response due to ε_o absorption and a modest response due to that in ε_e. This provides a baseline for comparison to the porous alumina layer. The plots shown are based on aluminum optical constants obtained by inversion of ellipsometric data [23]. Some noise from these measurements is seen in the response to absorption in ε_o.

Porous alumina. The optical model for porous alumina is effectively the same as silicon rods and wells, with the solid volume fraction more closely matching that of the rods discussed here. The structure, as seen in a previous publication [23], is more hexagonal, but often with imperfections, so the actual volume fractions fall somewhere between the two cases in Eq. (6). The response is similar to that of flat silicon in that absorptions in ε_e and ε_o give rise to opposing responses of similar shape. Distinguishing between these two would be difficult, but different incidence angle dependences make this plausible. Although the response to ε_o absorption is the largest of all the simulations, the response to ε_e absorption is relatively small. The porous structure has the distinct advantage of uniform spectral sensitivity, so that changes in ellipsometric spectra most closely match dielectric function properties of the adsorbate.

General comments. Although ρ gives an indication of how much more adsorbate can be condensed on a surface in a given area, the actual signal enhancement is likely to be somewhat less than ρ. For instance, the comparison between flat aluminum and the porous alumina [23] shows only about a factor of 3 increase in ellipsometric sensitivity (strongly dependent on incidence angle), while $\rho = 25$. However, the best ellipsometric signals on aluminum are observed for large incidence angles, which require larger sample areas and more total adsorbate. The proposed structures can give some guidance field in predicting what sensitivity enhancement can be achieved, but practical considerations such as this are best evaluated when the specific adsorption enhancement structures are known.

A concise summary of the properties and results of calculations presented in this paper for the various structures is shown in Table 2.

Table 2

Enhancement properties of proposed structures. Porous alumina and silicon trenches have favorable properties, with silicon trenches providing the best anisotropy information

Geometric structure	Properties
Bare aluminum	Simple interpretation, negligible o-ray sensitivity
Porous alumina	Simple interpretation, improved sensitivity (o and e)
Bare silicon	Low sensitivity, difficulty distinguishing o and e
Si rods	Modest sensitivity, little o–e distinction
Si well	Modest sensitivity, little o–e distinction
Si trenches	Good sensitivity and o–e distinction

5. Conclusion

A framework is presented for calculating the ellipsometric response of several geometric patterned structures with adsorbed material. The discussion has centered on infrared ellipsometry, but the same sensitivity analysis approach can be applied to visible ellipsometry, as long as the pattern dimensions are significantly smaller than the wavelength. Expressions for surface area enhancement and volume fractions of the solid, void, and adsorbed components are given. Calculations are performed for a dielectric (silicon) surface, metallic surface, silicon trenches, silicon rods, silicon wells, and porous alumina on aluminum. The models presented may be adapted to other biomaterials by adjusting the dimensions. The trench structure shows significant promise in both sensitivity to absorption and determination of anisotropy. Despite its lower dimensionality, its surface area enhancement is not much smaller than rod and well structures (Table 1). The porous matrix gives relatively good sensitivity and is spectrally uniform. The difficulty of using conventional ellipsometric parameters ψ and Δ alone to calculate and predict sensitivity to optical model parameters is noted. An alternative method using quantities more closely related to measured intensities is used.

These calculations were performed assuming protein adsorbs to the solid in a uniform layer with good coverage. Studies of porous alumina layers exposed to protein solutions [22] illustrate that some surfaces, due presumably to their chemical nature, do not adsorb proteins readily. Material selection or surface functionalization then become considerations in achieving higher sensitivity.

Sponegelike porous materials or fabricated structures such as logpiles with subsurface voids may also be able to yield increased volume fractions of protein, but these structures were not included here because of the increased difficulty of fabrication.

Acknowledgements

We wish to thank the U.S. Army for its financial support for this project via contract number W911NF-04-2-0011. Additional support was provided by the University of Nebraska-Lincoln by the Nebraska Research Initiative and the College of Engineering and Technology.

References

[1] H. Arwin, L.M. Karlsson, A. Kozarcanin, D.W. Thompson, T. Tiwald and J.A. Woollam, Carbonic anhydrase adsorption in porous silicon studied with infrared ellipsometry, *Physica Status Solidi C* (2005), accepted for publication.
[2] D.E. Aspnes, J.B. Theeten and R.P.H. Chang, Nondestructive characterization of interface layers between Si or GaAs and their oxides by spectroscopic ellipsometry, *Journal of Vacuum Science and Technology* **16** (1979), 1374–1378.
[3] R.M.A. Azzam and N.M. Bashara, *Ellipsometry and Polarized Light*, North-Holland Pub. Co., New York, NY, 1977.
[4] S. Bandyopadhyay, A.E. Miller, H.C. Chang, G. Banerjee, V. Yuzhakov, D.F. Yue, R.E. Ricker, S. Jones, J.A. Eastman, E. Baugher and M. Chandrasekhar, Electrochemically assembled quasi-periodic quantum dot arrays, *Nanotechnology* **7** (1996), 360–371.
[5] J. Chen, J.B. Anderson, C. DeWeese-Scott, N.D. Fedorova, L.Y. Geer, S.Q. He, D.I. Hurwitz, J.D. Jackson, A.R. Jacobs, C.J. Lanczycki, C.A. Liebert, C.L. Liu, T. Madej, A. Marchler-Bauer, G.H. Marchler, R. Mazumder, A.N. Nikolskaya, B.S. Rao, A.R. Panchenko, B.A. Shoemaker, V. Simonyan, J.S. Song, P.A. Thiessen, S. Vasudevan, Y.L. Wang, R.A. Yamashita, J.J. Yin and S.H. Bryant, MMDB: Entrez's 3D-structure database, *Nucleic Acids Research* **31** (2003), 474–477.
[6] M.J.A. de Dood, Silicon photonic crystals and spontaneous emission, PhD Dissertation, Utrecht University, 2002.
[7] A.C. Galca, E.S. Kooij, H. Wormeester, C. Salm, V. Leca, J.H. Rector and B. Poelsema, Structural and optical characterization of porous anodic aluminum oxide, *Journal of Applied Physics* **94** (2003), 4296–4305.
[8] A. Heilmann, *Polymer Films with Embedded Metal Nanoparticles*, Springer, Berlin, New York, 2003.

[9] G.E. Jellison, Spectroscopic ellipsometry data analysis: measured versus calculated quantities, *Thin Solid Films* **313** (1998), 33–39.
[10] O. Jessensky, F. Muller and U. Gosele, Self-organized formation of hexagonal pore arrays in anodic alumina, *Applied Physics Letters* **72** (1998), 1173–1175.
[11] R.P. Jia, Y. Shen, H.Q. Luo, X.G. Chen, Z.D. Hu and D.S. Xue, Photoluminescence spectra of human serum albumen and morin embedded in porous alumina membranes with ordered pore arrays, *Journal of Physics-Condensed Matter* **15** (2003), 8271–8279.
[12] B. Johs and C.M. Herzinger, Precision in ellipsometrically determined sample parameters: simulation and experiment, *Thin Solid Films* **455–456** (2004), 66–71.
[13] B. Johs, J.A. Woollam, C.M. Herzinger, J. Hilfiker, R. Synowicki and C.L. Bungay, Overview of Variable Angle Spectroscopic Ellipsometry (VASE), part II: Advanced applications, *Critical Reviews of Optical Science and Technology* **CR72** (1999), 29–58.
[14] L.M. Karlsson, P. Tengvall, I. Lundstrom and H. Arwin, Adsorption of human serum albumin in porous silicon gradients, *Physica Status Solidi A* **197** (2003), 326–330.
[15] L.M. Karlsson, R. Tengvall, I. Lundstrom and H. Arwin, Penetration and loading of human serum albumin in porous silicon layers with different pore sizes and thicknesses, *Journal of Colloid and Interface Science* **266** (2003), 40–47.
[16] V. Lehmann, Trends in fabrication and applications of macroporous silicon, *Physica Status Solidi A* **197** (2003), 13–15.
[17] L. Menon, Synthesis of nanowires using porous alumina, *Quantum Dots and Nanowires* (2003), 141–191.
[18] V. Mizeikis, H.B. Sun, A. Marcinkevicius, J. Nishii, S. Matsuo, S. Juodkazis and H. Misawa, Femtosecond laser microfabrication for tailoring photonic crystals in resins and silica, *Journal of Photochemistry and Photobiology A* **145** (2001), 41–47.
[19] M. Schubert, E. Franke, H. Neumann, T.E. Tiwald, D.W. Thompson, J.A. Woollam and J. Hahn, Optical investigations of mixed-phase boron nitride thin films by infrared spectroscopic ellipsometry, *Thin Solid Films* **313–314** (1998), 692–696.
[20] M. Schubert, Generalized ellipsometry and complex optical systems, *Thin Solid Films* **313–314** (1998), 323–332.
[21] B. Stuart and D.J. Ando, *Biological Applications of Infrared Spectroscopy*, Published on behalf of ACOL (University of Greenwich) by John Wiley, New York, 1997.
[22] D.W. Thompson, Enhanced infrared ellipsometry for adsorbed proteins, PhD Dissertation, University of Nebraska-Lincoln, 2004.
[23] D.W. Thompson, P.G. Snyder, L. Castro, L. Yan, P. Kaipa and J.A. Woollam, Optical characterization of porous alumina from vacuum ultraviolet to mid-infrared, *Journal of Applied Physics* **97** (2005), accepted for publication.
[24] H.G. Tompkins and E.A. Irene, *Handbook of Ellipsometry*, William Andrew Pub., Norwich, NY, 2005.
[25] J.A. Woollam, B. Johs, C.M. Herzinger, J. Hilfiker, R. Synowicki and C.L. Bungay, Overview of Variable Angle Spectroscopic Ellipsometry (VASE), part I: Basic theory and typical applications, *Critical Reviews of Optical Science and Technology* **CR72** (1999), 3–28.
[26] F. Wooten, *Optical Properties of Solids*, Academic Press, New York, 1972.